Self-Organization in Dendrimer Polyelectrolytes

K. Karatasos

Chemical Engineering Department, Physical Chemistry Lab, Aristotle University of Thessaloniki, 54124 Thessaloniki, Greece

Received August 29, 2007; Revised Manuscript Received December 30, 2007

ABSTRACT: Results from molecular dynamics simulations are reported, describing self-organization in solutions of charged dendrimer molecules upon variation of the strength of the electrostatic interactions, in the presence of explicit solvent and counterions. Systems of two sizes bearing different surface charge densities are studied at constant temperature and volume conditions. It is found that a systematic variation of Bjerrum length triggers a mechanism associated with counterion spatial correlations, which drives the systems from an amorphous liquidlike arrangement to an ordered state bearing the symmetry of a cubic phase. The role of dendrimer interpenetration, trapping of counterions, and solvent depletion in the ordering process is also explored. As this study employs a description which takes into account all the principal internal degrees of freedom of dendrimer molecules, the conclusions drawn are expected to offer a fair description of the behavior of realistic systems bearing similar dendritic topology.

I. Introduction

Dendrimers are treelike functional nanosized molecules for which the recently developed synthetic protocols enable a molecular-level engineering of features like size, shape, topology, flexibility, and surface chemistry.[1,2] Because of their intermediate nature between polymers and colloids,[3] properties of both of these classes of materials can be combined in dendrimers in a controlled manner. Their practically monodisperse nature and their high functionality render them promising building blocks to form special supramolecular structures and very unique microenvironments.[4−6]

Their potential to form such structures by modification of their chemical details and by adjusting their thermodynamic environment has been documented nearly two decades ago[7] and has since been exploited in a wide range of applications, from nanoengineering of electronic devices through directed self-assembly[8] to novel applications in medicine and biotechnology.[9−11] Apart from the structural information "programmed" into their architecture which can act as a molecular-level recognition process to trigger self-assembly,[12,13] as in other polymeric systems bearing ionizable groups self-organization is at a large extent driven by the electrolytic behavior of these materials.[14]

Despite the increasing scientific and industrial interest in supramolecular assemblies of dendritic materials, only few theoretical and simulational studies have so far addressed the self-organization of such systems, in principle employing coarse-grained models or rather small in size and simple in structure molecules.[15−17] Significant progress has however been made in the description of systems that bear resemblance in certain aspects to dendrimer molecules. Recent theoretical studies and computer simulations in charged colloids (including macroions of different geometries, size, surface charge density) or colloidal-like polymeric models (e.g., multiarm star polymers, micelles, spherical brushes) in different thermodynamic conditions have advanced our understanding on precesses associated with formation of macroion assemblies.[18−22] Mechanisms that have been investigated such as complexation with other charged moieties, counterion condensation, overcharging, and like-charge attraction are known to play a key role not only in novel applications but also in the function of many biological systems.[23,24]

In several of these studies, the traditional Poisson−Boltzmann (PB) theory and its linearized Debye−Hückel (DH) version[25] have been proven inadequate to describe electrostatic phenomena met in colloids and biological systems.[26,27] Particularly when existence of strong electrostatic interactions promotes effects like charge inversion, attractions between similar charges and ion correlations.[24,25,28,29] As far as these efforts have progressed, the elementary mechanisms for self-assembly and complexation in strongly charged electrolyte systems are considered to be only partially understood.[30] Even more so, since attributes characterizing realistic systems such as a nonuniform surface charge density, deformable shape, explicit solvent, and interpenetration between different molecules are usually treated in a simplified or implicit manner or even not considered at all. Therefore, examination of models bearing details which enable a closer comparison to real systems is expected to contribute toward a deeper understanding of the experimentally observed behavior and ultimately to the prospect of controlling the emerging structures and their physical properties.

To this end, we have conducted molecular dynamics simulations in order to examine mechanisms involved in the self-organization of dendrimer polyelectrolytes in explicit-solvent solutions, under the influence of varying strength of electrostatic interactions, and for models bearing different size and surface charge densities.

II. Model and Simulation Details

As we were interested in exploring generic rather than specific characteristics arising from the dendritic topology, the dendrimer molecules were modeled in the united atom (UA) representation. The structure considered starts from a trifunctional core and grows radially outward with branching functionality (f) equal to 3 and two spacer bonds between branching points as schematically shown in Figure 1. The concentric circles in the schematic denote the different generational shells (g). According to the adopted topology, the number of beads per dendrimer molecule as a function of the generational shell index g (starting from 0) is given by $N(g) = 1 + 6 \times [2^{g+1} - 1]$. The maximum number of shells define the generation G of the dendrimer. Following our previous work,[31] each UA was assigned mass corresponding to a CH_i group, where i is determined by the

10.1021/ma7019489 CCC: $40.75
Published on Web 01/15/2008

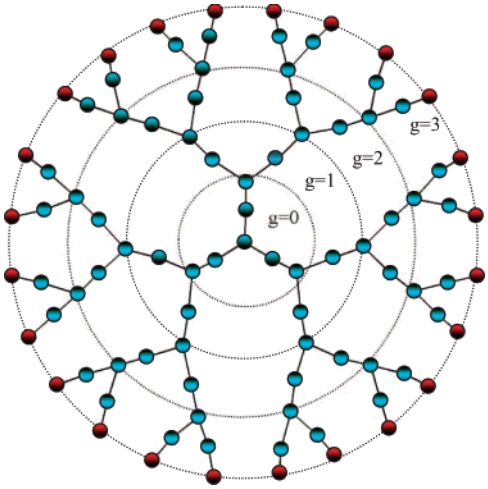

Figure 1. Schematic representation of a dendrimer model of generation 3. The circles denote the boundaries of each generational shell (*g*). The charged terminal beads are shown in red.

connectivity of each bead, while each solvent molecule was represented by a UA CH_4 group.

Systems of generations $G = 3$ and $G = 4$ were simulated by means of molecular dynamics (MD) simulations under the constant-temperature, constant-volume (NVT) thermodynamic ensemble.[32] The models were placed in cubic simulation boxes (with application of periodic boundary conditions) and comprised by 30 dendrimer molecules having their terminal beads single-charged, the required number of monovalent counterions to preserve overall electrical neutrality (720 for G3 and 1440 for G4) each bearing the same mass as that of a charged dendrimer bead, and an appropriate number of neutral solvent beads (1086 for G3 systems and 2300 for G4) in order to bring G3 and G4 systems at the same density. Charging of the terminal beads only is analogous, e.g., to the situation met in neutral pH solutions of amine-terminated (like polyamidoamine) dendrimers where only protonation of the primary (terminal) amines takes place.[33]

The so-constructed models assumed a polymer volume fraction of ≃10%, corresponding to a concentration of ≃$0.1C^*$, where C^* represents the overlap concentration. It was chosen for the systems to be constructed at concentrations well below C^* in order to avoid intervention of kinetic/jamming phenomena. The interaction potential adopted for the dendrimer molecules consisted of bonded terms (bond stretching, bending angles, and torsions) and nonbonded interactions of the Lennard-Jones (LJ) type (with a 10 Å cutoff), following the parametrization of the DREIDING force field.[34,35] LJ parameters for nonlike pairs were calculated as arithmetic ($\sigma_{ij} = (\sigma_i + \sigma_j)/2$) or geometric ($\epsilon_{ij} = \sqrt{\epsilon_i \epsilon_j}$) means of the individual parameters. For charged beads pairs, only the repulsive part of the Lennard-Jones potential was considered (the LJ potential was cut at $r_c = 2^{1/6}\sigma$ and shifted to zero). Electrostatic interactions were taken into account via a full Ewald summation scheme.[36] Hydrogen-bonding and solvent polarity terms[37] are not considered explicitly. In order to use units pertinent to characteristic parameters of the models, henceforth energy and length will be expressed in terms of the LJ interaction parameters ϵ and σ between two charged beads, respectively, while time will be measured in units of $\tau = \sigma\sqrt{m/\epsilon}$, where m represents an average mass of a dendrimer bead. To retain consistency with and allow comparison to results of past studies that have examined analogous dendrimer models,[31,38] temperature was defined by $\epsilon = 0.3k_BT$ (corresponding to Θ-conditions for linear polymer analogues[31]), where k_B represents Boltzmann's constant. For integration of the equations of motion the velocity Verlet algorithm was used, with a time step $\Delta t \cong 7 \times 10^{-4}\tau$. After construction of the initial configurations by the aid of the amorphous cell algortihm,[39] the models underwent 50 000 energy minimization steps by steepest descent and conjugate gradient methods, followed by an MD equilibration in the constant-volume, constant-temperature (NVT) ensemble of 10^6 steps, after which the systems have reached a stable state in terms of energetic (total energy, Coulombic energy, and Coulombic virial) and conformational characteristics (i.e., radii of gyration of the dendrimer molecules, arrangement of ions and solvent molecules around dendrimers). Production runs were then performed, generating trajectories of $\sim 2 \times 10^3\tau$. For each generation G, a number of systems were examined at constant density and temperature but varying the strength of the electrostatic interactions.

A measure for the relative importance of the electrostatic interactions in a polyelectrolyte solution in the DH approximation is the Debye screening length κ^{-1}

$$\kappa^{-1} = \frac{1}{\sqrt{4\pi l_B \sum_i c_i z_i^2}} \tag{1}$$

where c_i and z_i refer to the concentration and the charge of ith species of ions in the solution. l_B symbolizes the Bjerrum length, defined as

$$l_B = \frac{e^2}{4\pi\epsilon_0\epsilon_r k_B T} \tag{2}$$

This length corresponds to the separation between two charges, at which the Coulombic interaction is comparable in magnitude to the thermal energy. In the former expression, e is the electron unit charge, ϵ_r is the relative dielectric permittivity, and ϵ_0 stands for the dielectric permittivity of the vacuum. For instance, l_B of water (with $\epsilon_r \simeq 80$) at room temperature is ∼7 Å, which is close to 2 in the units of our models. In the context of the DH approximation, as implied by eq 1, in actual experiments apart from temperature the relative strength of electrostatic interactions can be controlled either by changing the number density or the valency of the ions (e.g., by controlling the charging level of the dendrimer and the salt concentration[40−42]) or through modification of the Bjerrum length by selecting solvents which bare relatively high or low dielectric permittivities.[43−45] In this work, it was chosen that the number densities and the charge of the ions remain constant, while changes in the strength of electrostatic interactions were introduced by means of a systematic variation of l_B. The values of Bjerrum lengths examined ranged from 0.5 to 150 (in units of σ), which would correspond to a variation of κ^{-1} between 0.74 and 0.04 σ in the context of the DH theory for the examined models. An approximate mapping to real units arising from a comparison between the radii of gyration of our models (see section III) to the size of PAMAM dendrimers with only the primary amines protonated[46] yields a length of 3.3 Å for the simulation unit.

An example of a G4 equilibrated system at $l_B/\sigma = 1$ is shown in Figure 2. Apart from the systems corresponding to the lower values of l_B examined, initial configuration of systems at higher Bjerrum lengths were taken by the final configurations of the runs simulated at the immediately "neighboring" (smaller) value of l_B. To check whether starting configurations could influence the obtained results, a number of runs at high Bjerrum lengths

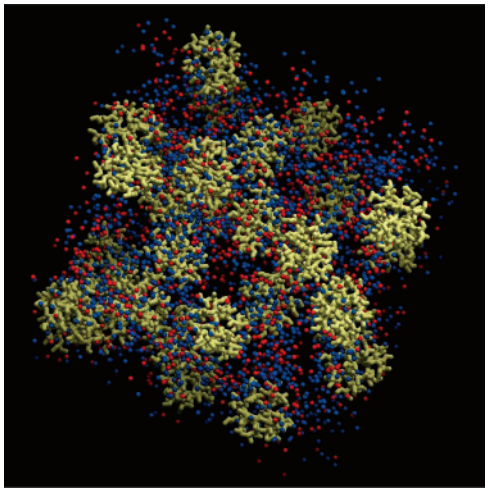

Figure 2. Snapshot of an equilibrated G4 model at $l_B/\sigma = 1$. Red beads indicate counterions while blue beads represent the solvent.

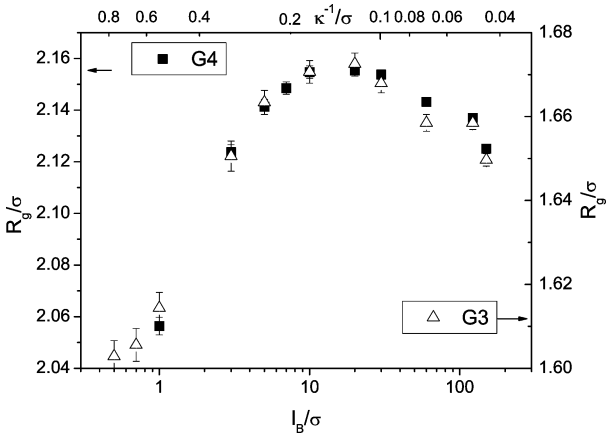

Figure 3. Dependence of the radius of gyration on Bjerrum length for the two generations studied. The top *x*-axis represents the screening length according to the DH approximation and is linked to the corresponding l_B values of the G3 model.

were also initiated by final configurations of systems of much smaller l_B. As was found, the "relaxation" of these systems from a "quenched" low-l_B configuration to the equilibrium state was a rapid process (of the order of a few τ); therefore, no separate discussion for these runs will be made. In addition, indicative runs at somewhat lower concentrations for both models showed no qualitative differences from the picture presented here.

III. Effects on the Size of the Dendrimers

Previous computer simulation studies in single-dendrimer models[38,47] have illustrated a nonmonotonic dependence of the size of the dendrimer with the strength of electrostatic interactions. This behavior was attributed to the presence of counterions and the interplay between repulsive interactions of the like-charged dendrimer beads and the attractive forces between the latter and the oppositely charged ions. In the case of our multidendrimer models an analogous pattern is also observed as shown in Figure 3, bearing though distinct features compared to the single-dendrimer behavior.

The peak in the R_g vs l_B dependence in the present systems occurs at larger l_B/σ value, while the maximum relative change in dendrimer dimensions with respect to the neutral models[35] amounts only to about 1.2% for G3 and 2.5% for G4 systems, in contrast to corresponding relative changes of about 12%[38] and almost 20%[47] observed in the single-dendrimer models. Although certain dissimilarities in the dendritic topology between the models may partly be responsible for this discrepancy, the fact that the single-dendrimer systems were represented by bead−spring freely jointed models, lacking therefore force field terms associated with other degrees of freedom, could be the main reason for the observed differences. This notion is corroborated by the fact that single-dendrimer runs of the G3 model (not shown here) yielded an R_g vs l_B dependence similar to the one depicted in Figure 3.

It should also be noted that the locus of the peak is independent of the size of the examined models. A mechanism consistent with the observed behavior involves[38] (i) a swelling of the dendrimers at low l_Bs due to mutual repulsion of the like-charged terminal beads and (ii) an effective contraction of the dendrimer from the swollen state at high l_B values, driven by gradual counterion condensation which can effectively screen the like-charge repulsion of the terminal beads and allow the dendrimer to reach its original size. It must also be considered that many-body interactions between different dendrimers and between dendrimers and their neighboring counterions can play a role in this process affecting thus their conformational characteristics.[17,48] Although the observed relative change in dendrimer dimensions upon alteration of the strength of electrostatic interactions (in the examined range) is rather moderate (about 3.5% for G3 and 5% for G4 systems taking as a reference the value of R_g corresponding to $l_B/\sigma = 1$), it may well be significant in targeted drug-delivery applications where a well-controlled release mechanism is desired.[49,50]

IV. Spatial Arrangement of Dendrimer Molecules

Alongside with the change in the dimensions of the dendrimer molecules, significant structural rearrangements take place within the solutions upon modification of l_B. To follow these changes, we have examined the static structure factor arising from the centers of mass of each dendrimer. Instead of employing the formula describing isotropic media,[51] we have resorted to an expression that makes no assumption as to the isotropy of the studied system[25]

$$S(q) = \left\langle \left\langle \frac{1}{N} \left| \sum_{i,j}^{N} e^{i\vec{q}\cdot\vec{r}_{ij}} \right|^2 \right\rangle_q \right\rangle_{\text{directions}} \tag{3}$$

N is the number of "scatterers" (here the number of dendrimer molecules), and indices i,j refer to a pair of them. For each scattering vector studied with magnitude q, $S(q)$ was calculated as an average over 50 orientations of vector $\vec{q}$ uniformly distributed over a surface of a sphere.[52] The evolution of $S(q)$ for different l_Bs and for the two dendrimer generations is illustrated in Figure 4. For clarity, *y*-axis values of each curve are shifted by a factor of 0.5 compared to the preceding one. Comparison of the general behavior of the structure factors between the G3 and the G4 systems shows that besides some differences related to the specific locations of the observed peaks, it appears to follow a common pattern. At the lower q range a low-amplitude peak (referred to as p1 from now on) develops with an approximately l_B-independent q location. The main intermolecular scattering peak corresponding to first neighbors (referred to as p2) shifts to larger q magnitudes, signifying a strong dependence of the spatial rearrangement of molecules on the strength of electrostatic interactions. Moreover, while at low-l_B values the structure factors essentially reflect amorphous systems (the arrows at low-l_B spectra denote the peak locations expected for a liquidlike arrangement), at larger Bjerrum lengths additional peaks appear, indicating emergence of structural order. Appearance of "prepeaks" analogous to p1

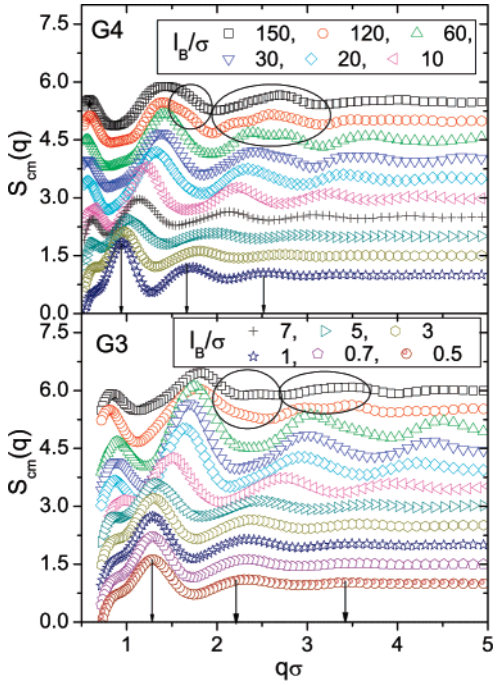

Figure 4. Static structure factors arising from the centers of mass at different values of l_B for the G3 (lower panel) and the G4 (upper panel) dendrimer models as a function of the magnitude of the scattering vector. Each curve is shifted in *y*-axis by 0.5 for clarity of presentation. Circles and ellipses emphasize the emergence of new peaks at high l_Bs.

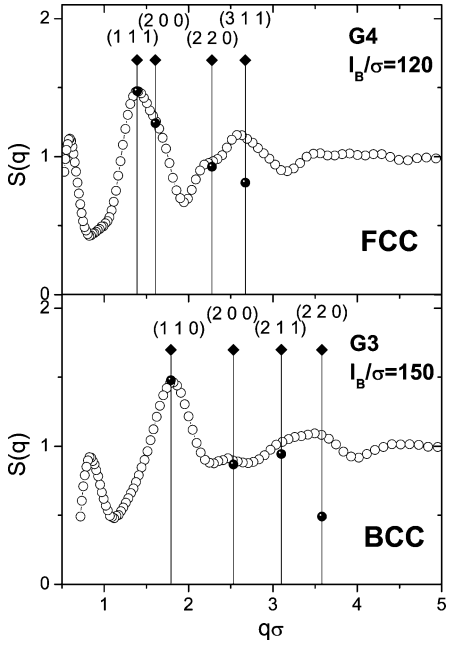

Figure 5. Static structure factors arising from the centers of mass at elevated strength of electrostatic interactions for the examined models. Vertical lines denote the locations corresponding to the high-intensity diffraction peaks for a face-centered cubic (upper panel) and a body-centered cubic (lower panel) lattice. Miller indices of the corresponding scattering planes are shown on top of each line. Solid spheres represent the expected relative amplitudes of each peak with respect to that of the larger maximum.

has been reported in the literature at scattering spectra of diverse systems such as glasses,[53,54] ionic liquids,[55] and polyelectrolyte models.[18] These low-*q* maxima have been attributed to different possible origins, like "chemical ordering"[53,54] related to ordering of interstitial voids around formed clusters or specific molecular moieties, spatial correlations between such formed clusters,[56] "Coulombic ordering"[55] associated with spatial ion correlations, and competition of different length scales characterizing the examined systems.[18] In our case, the position of p1 is incompatible with a distance which is an integer multiple of that corresponding to the location of p2 and to the size of the simulation box. It appears therefore to be consistent either to a gradual development of extended range order associated with a "clustering" mechanism of dendrimer molecules or to the "Coulombic ordering" scenario.

The spatial rearrangements taking place at the large-l_B regime actually result to ordering of the examined systems in cubic phases described by the symmetry of bcc and fcc lattices for G3 and G4 systems, respectively, as shown in Figure 5.

The vertical lines denote the positions corresponding to the principal scattering planes of bcc (for G3) and fcc (for G4) structures (in parentheses are the Miller indices of these planes). The solid sphere points mark the relative scattering amplitudes expected for these structures.[57] Evidently, not only the locations of the peaks but also their relative amplitudes corroborate the identification of the nominal lattice symmetries. The deviation of the relative amplitudes of the higher-*q*/lower-intensity peaks from those expected for the corresponding perfect crystalline structures can be interpreted as an indication of lattice imperfections and/or as a coexistence of crystalline and amorphous domains.[58] The ordered structures are illustrated in Figure 6, where a snapshot of the simulation box for each system is shown together with periodic images of it. To quantify the gradual change of the packing of dendrimer molecules in the solutions, we have followed the position of p2 (denoted as q^*) and plotted it as a function of l_B for the examined models, as shown in Figure 7.

Three characteristic regimes can be distinguished in the dependence of q^* as a function of Bjerrum length. In regime I, which can be considered as a weak electrostatic interactions region, q^* remains rather insensitive to l_B changes. The lower bound of region II signifies the onset of a stronger coupling regime (e.g., in the context of the strong coupling theory[59,60]) between the dendrimer (macroion) and the counterions, within which a "transition" in dendrimer spatial arrangement takes places. This gradual change is manifested as a monotonic increase of q^* as a function of l_B (i.e., the dendrimer molecules approach each other on average) toward a plateau value. Regime III is defined by the start of this leveling-off behavior.

V. Condensation of Counterions and Solvent Depletion

To explore the role of the counterion condensation mechanism to this structural transition, we can monitor the actual number of counterions that are "adsorbed" on the surface or trapped within the dendrimer molecules during this process. To accomplish this, we have constructed the distributions of the dendrimer beads as well as those of the counterions with respect to each dendrimer's center of mass. Next, we have calculated the number of bound charges by integration of the ion bead distributions up to the point where the dendrimer and the ion distributions overlap. An example of such distributions is depicted in Figure 8 for the G4 systems in two l_B values corresponding to regimes I and II as discussed earlier. For the dendrimer molecules, apart from the overall distributions (i.e., including all the beads), distributions of beads belonging to the outer generational shell where the charged beads are located are shown as well. Apparently, upon increase of l_B, the degree of overlap between dendrimer and ion distributions increases. The small peaks appearing in the distribution of beads of the terminal dendrimer generation and that of the counterions at

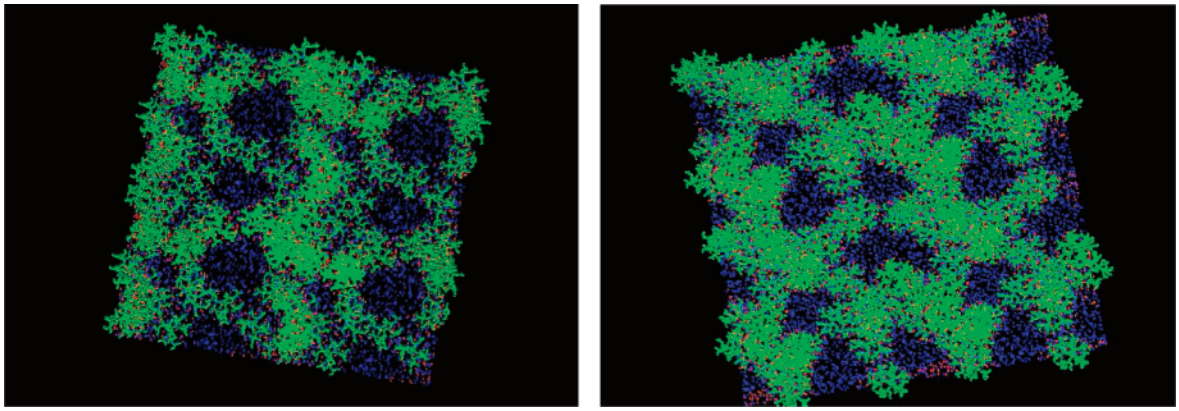

Figure 6. Ordered phases (left for G3 and right for G4 model) at the l_Bs appearing in Figure 5 for each model. The simulation box is shown together with periodic images to facilitate the visual identification of the formed structures.

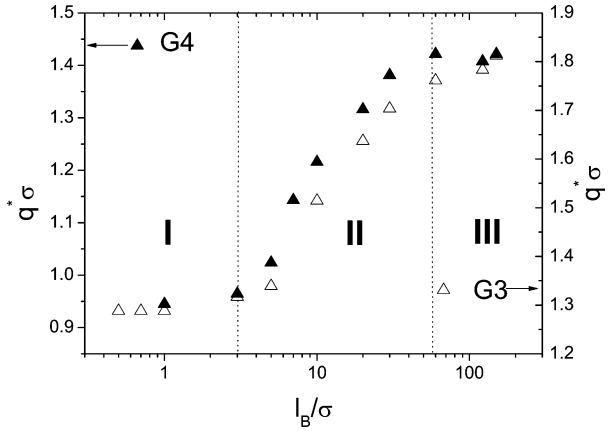

Figure 7. Bjerrum length dependence of the magnitude of the scattering vector corresponding to the principal maxima appearing in Figure 4. Vertical lines define the boundaries of the three regimes according to the observed behavior.

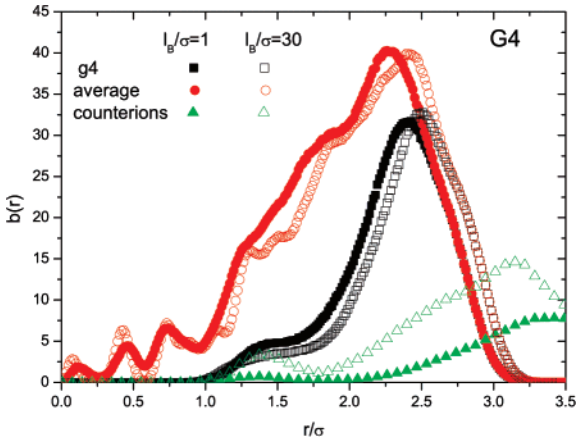

Figure 8. Number distributions with respect to the center of mass of the dendrimer, of all dendrimer beads and of those belonging to the outer generational shell of the G4 dendrimers, together with the respective counterion distributions. Distributions are shown at two l_B values belonging to regimes I and II as defined in Figure 7.

high l_B are due to the backfolding effect.[31] This effect is responsible for the fact that a certain number of counterions are attracted (and practically trapped) at the interior of the dendritic structure since a number of oppositely charged dendrimer beads are folded back toward the dendrimer center.

The so-calculated number of bound counterions (normalized with the total number of charged beads per dendrimer) is shown for the two examined models in Figure 9. The inset displays

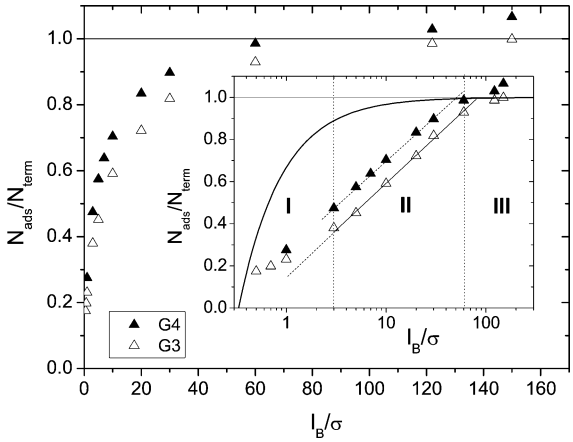

Figure 9. Main panel: "condensation curves" indicating the number of bound counterions relative to the total number of charged beads per dendrimer molecule. The horizontal line marks the limit of electrical neutrality. Inset: semilogarithmic representation of the curves appearing in main panel. Vertical lines indicate the boundaries between the three regimes as defined in Figure 7. Horizontal line marks the neutrality limit. The thick solid curve denotes a theoretical prediction for counterion condensation on a linear polyelectrolyte[61] as described in the text.

the same curves in a semilogarithmic format. The vertical dotted lines denote the boundaries of the three regimes of l_B as defined in Figure 7. The thick solid curve shows the behavior predicted from the Manning theory[61] including finite length corrections[62] for a linear polyelectrolyte at the dilute regime, bearing the same radius of gyration as that of the G3 model. The behavior of the "condensation curves" for the two systems share some common features but bear certain differences as well. As shown in the inset, for both dendrimer systems the curves seem to follow a logarithmic law in regime II. Evidently, this behavior cannot be reproduced by the standard Manning prediction even if the finite length of the linear model is also considered. Such logarithmic dependence at an intermediate regime of Bjerrum lengths is compatible with more recent self-consistent theoretical calculations for the counterion condensation in flexible linear polyelectrolytes, when effects like the translational entropy of adsorbed and unadsorbed counterions and correlation among ion pairs formed by adsorbed counterions on the polymer chain are taken into account.[63] Deviations from the logarithmic dependence at very low and very large values of l_B which are described for linear polyelectrolytes[63] are observed for the dendrimer systems as well (regions I and III).

In the dendrimer models of the fourth generation possessing the higher surface charge density (~25% higher compared to

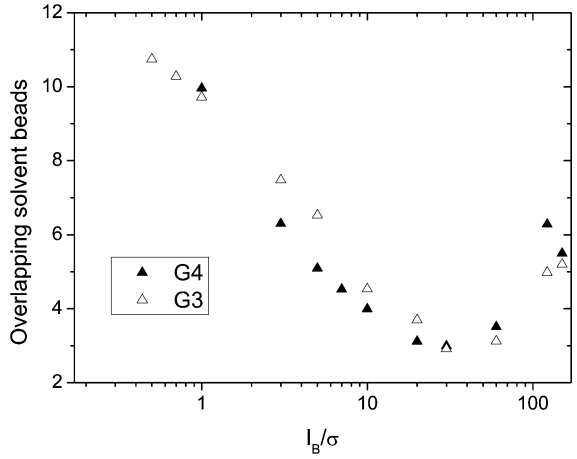

Figure 10. Number of solvent beads found within the limits of the overall dendrimer bead distributions for G3 and G4 models as a function of l_B.

G3 systems) counterion condensation proceeds "faster" in the sense that at constant l_B a larger fraction of counterions is bound compared to the one corresponding to the G3 models. Moreover, while at the high l_B limit in G3 systems the number of bound counterions is exactly the one required for counterbalancing the opposite dendrimer charge (i.e., resulting on average to neutral dendrimer−counterion complexes), the corresponding curve of the G4 systems overcomes the neutrality limit (the error margin is estimated to be of he order of the symbols' size). While at first glance this might seem counterintuitive since the total number of counterions exactly matches that of the total number of charged dendrimer beads, an explanation is in order if dendrimer molecules come sufficiently close so that their bead and their corresponding counterion distributions start overlapping. In this case an additional number of counterions which serves for neutralizing charged beads of the neighboring dendrimers will be present. This extra number becomes significant only when the degree of dendrimer overlap becomes sufficiently high. Although such so-called overcharging phenomena of macroions are commonly met in the presence of multivalent counterions,[64] charge inversion has also been predicted in the presence of monovalent counterions at high ionic concentrations.[65,66] Interpenetration of dendrimer molecules is a mechanism that can account for such elevated local counterion concentrations.

The analogous picture concerning the beads of the solvent that remain in the vicinity of a dendrimer molecule (following the same procedure of overlapping distributions) is shown in Figure 10 for the examined systems.

The pattern followed is common for both generation dendrimers. Similarly to the behavior of the radius of gyration (Figure 3), a nonmonotonic dependence is noted, exhibiting a minimum practically at the same abscissa as that at which the dendrimers assume their larger dimensions. This behavior can be attributed to energetic reasons since such a solvent depletion mechanism (upon increase of l_B) increases the entropy, influencing thus the systems' equilibrium state at each l_B. At the absence of this contribution to free energy, the interplay between attractive and repulsive electrostatic interactions between charged dendrimer beads and counterions (which essentially determine the dendrimer dimensions) might have resulted to maximization of the dendrimer size at a different l_B than the one observed. In this context, a link between the solvent rearrangement close to the dendrimers and the dendrimers' conformational characteristics is in order.

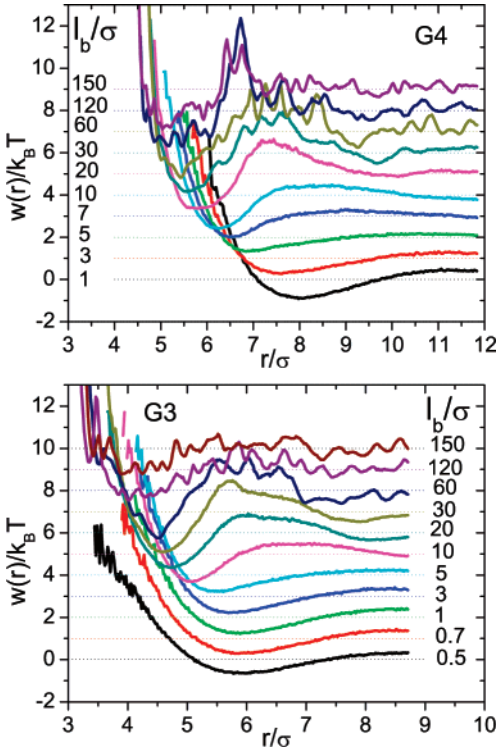

Figure 11. Potential of mean force (see text) for both the dendrimer sizes and for all the examined Bjerrum lengths. Curves are shifted by 1 in *y*-axis for better visual inspection.

VI. Role of Counterion Correlations in Dendrimer Interactions

In order to gain a better insight regarding the nature of the mean interaction between two dendrimer molecules, we have calculated the pair potential of mean force[17,67] $w(r)$ which is directly related to the radial distribution function $g(r)$ in the NVT ensemble.[68] Although in this approach counterion correlations and many-body interactions are not taken explicitly into account, it has been shown to provide a sound qualitative picture for the effective pair interaction in systems of charged macroions.[69,70]

$$g(r) = e^{-w(r)/k_BT} \tag{4}$$

Here $g(r)$ represents the radial distribution function arising from the centers of mass of the dendrimers. Figure 11 displays the evolution of $w(r)$ as a function of l_B for both generation systems. Each curve is shifted in *y*-axis by 1 with respect to the previous one for clarity. Even at the lower Bjerrum lengths, $w(r)$ indicates a weak attraction between the dendrimers. Attraction between like-charged macroions (e.g., colloids, proteins) has been predicted and described by several approaches and simulations,[26,27,60,71,72] while it has been experimentally observed as well.[20,73,74] As indicated in Figures 8 and 9, dendrimers in the low-l_B regime (I) attract a moderate number of counterions which suffices only for a partial screening of their charges. Moreover, the counterions and the terminal beads (and thus the total charge of the dendrimer) can be nonuniformly distributed. It has been reported that such nonuniform charge distributions are able to produce attraction between like-charged macroions.[28,29] At a higher l_B range (regime II) a stronger close-range attraction is developed accompanied by a midrange repulsion, while at the highest examined l_B values (regime III) an oscillatory behavior is observed indicative for the ordered dendrimer structure. Under conditions of strong electrostatic

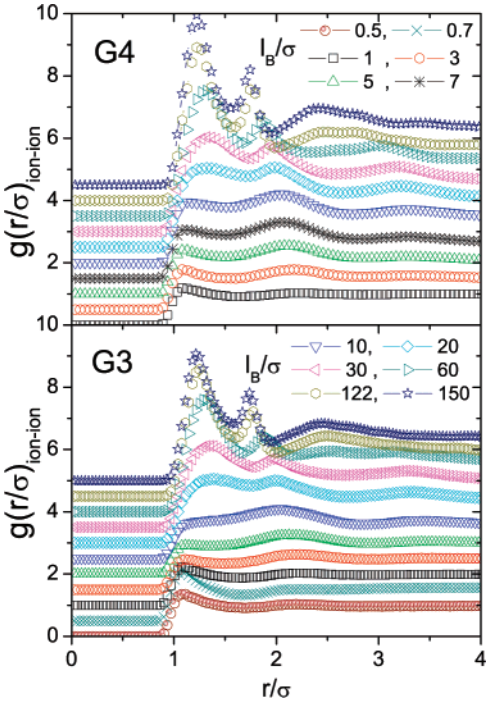

Figure 12. Radial distribution functions of the counterion beads for models of both generations and for all the examined l_B values. Each curve is shifted by a factor of 0.5 in *y*-axis with respect to its previous.

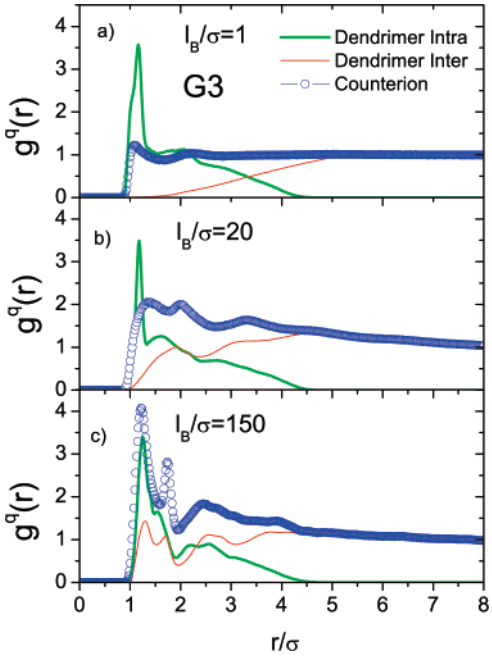

Figure 13. Comparison of the intra- and intermolecular contributions of the radial distribution functions of the charged dendrimer beads, with the corresponding distributions of the counterions for the G3 model, and for l_B values representing all three regimes of Coulombic coupling as defined in Figure 7.

interactions where counterion condensation takes place, close-range attraction between like-charged macroions can arise due to spatial correlations of the condensed counterions.[24,25,75−77] In solutions of charged sphere systems with their counterions, a similar short-range attraction followed by a midrange barrier in the potential of mean force was noted,[78] while in recent simulational studies attraction at short distances followed by repulsion at longer separations was also observed at highly charged colloidal particles with van der Waals interactions present.[70] Moreover, in the strong Coulombic coupling regime, existence of an energy barrier for counterion migration between neighboring charged spheres (which would promote attraction between the two like-charged macroions) was observed and attributed to the gain of correlation energy of counterions near the surface.[28] Combination of short-range attraction with partially screened (and thus of longer range) Coulombic repulsion can actually provide a stabilization mechanism of the dendrimer supramolecular structures, in a way similar to that described for globular protein clusters.[56]

To verify the existence of such correlations in the counterions' spatial arrangement, we have examined their radial distribution functions. Figure 12 presents these distributions for both systems.

As the intensity of the electrostatic interactions increases, different peaks appear with growing amplitude until at the high-l_B limit they assume a much sharper shape, indicating the presence of a layered (ordered) ionic arrangement. To identify the characteristic distances appearing in the counterion distributions, it is informative to compare them with those corresponding to the charged dendrimer bead pairs. For the calculation of the latter, we have distinguished between intra- and intermolecular contributions in order to assess in more detail the origin of the observed peaks. This comparison is described in Figure 13 for l_B values belonging to the three formerly identified regimes, for one of the examined generations. The picture characterizing the other generation's behavior is in complete analogy to the one shown. At low l_B where existence of strongly coupled dendrimer bead−counterion pairs is absent, the distributions are featured with peaks that would describe to a good approximation an uncharged dendrimer or a nonionic liquid, with their locations shifted to moderately longer distances due to the Coulombic repulsions. In the intermediate l_B range, however (Figure 13b), where Coulombic coupling is stronger, the counterion distributions become strongly correlated to the ones of the charged dendrimer beads, behaving almost as a superposition of the intra- and intermolecular contributions of the latter. This trend is clearly enhanced at the strongest coupling regime (Figure 13c). Although layering effects of monovalent ions near the surface of isolated charged spherical particles have been reported,[66] in the case of dendrimers one must emphasize the significant role of the intermolecular dendrimer charged pairs which to a large degree determine the equilibrium spatial arrangement of the counterions, either close to the dendrimer surface ($r/\sigma \leq 2$) or at longer distances.

VII. Summary and Conclusions

In this work we explored the response of peripherally charged dendrimer molecules upon change of the strength of electrostatic interactions, in low concentration solutions with the presence of explicit solvent and counterions.

Because of their characteristic architecture, these molecules behave in several aspects like soft colloidal particles, but what clearly distinguishes them from such systems is their internal degrees of freedom. It was demonstrated that characteristics arising from their distinct topology, like the backfolding of beads belonging to outer generations, the internal cavities that can "host" (or deplete) counterions and solvent molecules under appropriate conditions, their deformability that can allow shape fluctuations and thus anisotropic charge distributions, and their ability to interpenetrate, can drastically influence their behavior. On the other hand, although manifested in ways particular to the dendritic structure, mechanisms observed in colloidal systems such as counterion condensation, attraction of like-

charged molecules, and spatial counterion correlations are also present in dendrimer solutions.

For both the models studied (bearing different surface charge densities and molecular size) the aforementioned mechanisms were responsible for a development of counterion-mediated attraction between dendrimer molecules. Increase of the strength of electrostatic interactions resulted in a pair potential of mean force characterized by a short-range attraction and a longer-range repulsion which at the strong Coulombic coupling limit triggered a self-organization of dendrimers in cubic phases. For models with differences in size and in surface charge densities, the emerged structures assumed distinct symmetries, namely that of a bcc (for the G3) and that of a fcc (for the G4) structure. These structural differences between the two models affect their conformational characteristics, which are known to influence the degree of interpenetration between neighboring molecules and the backfolding effect,[35,51] modifying thus the geometric distribution of charge and the ability of solvent penetration into the dendrimer interior. In the present study, care was taken for a fair representation of dendrimer conformational characteristics by employing a detailed force field through which degrees of freedom like bond stretching, angle bending, and torsional rotation were explicitly considered. We must also note that it is not expected that the picture presented in this work (particularly the effects related to the observed counterion condensation mechanism) would be significantly affected by finite size effects. This notion is supported by the fact that the mechanisms involved in the self-organization process were found to be in complete analogy between the G3 and the G4 models which are at the same volume fraction but at distinctly different volumes. (The simulation box volume in G4 dendrimers was more than 250% larger compared to that of the G3 models.)

Although the parameter space pertinent to dendrimer self-assembly in solutions is far from being fully explored by the present study, it is believed that several of the mechanisms described are generic to the dendritic structure and may serve as a reference point for the interpretation of electrostatically driven self-ordering phenomena, in systems bearing topology similar to the examined models.

Acknowledgment. Funding from the Greek General Secretariat for Research and Technology under the framework of the PENED 2003 program (Grant No. 03EΔ716) is gratefully acknowledged. Part of this work was carried out under the HPC-EUROPA project (RII3-CT-2003-506079), with the support of the European Community-Research Infrastructure Action under the FP6 "Structuring the European Research Area" Programme. The author thanks Prof. Ch. Likos for valuable comments on the manuscript.

References and Notes

(1) Frechet, J. *Proc. Natl. Acad. Sci. U.S.A.* **2002**, *99*, 4782.
(2) Gittins, P.; Twyman, L. *Supramol. Chem.* **2003**, *15*, 5.
(3) Harreis, H. M.; Likos, C. N.; Ballauff, M. *J. Chem. Phys.* **2003**, *118*, 1979.
(4) Percec, V.; Cho, W.; Moller, M.; Prokhorova, S.; Ungar, G.; Yeardley, D. *J. Am. Chem. Soc.* **2000**, *122*, 4249.
(5) Corbin, P.; Lawless, L.; Li, Z.; Ma, Y.; Witmer, M.; Zimmerman, S. C. *Proc. Natl. Acad. Sci. U.S.A.* **2002**, *99*, 5099.
(6) Smith, D.; Hirst, A.; Love, C.; Hardy, J.; Brignell, S.; Huang, B. *Prog. Polym. Sci.* **2005**, *30*, 220.
(7) Tully, D.; Wilder, K.; Frechet, J.; Trimble, A.; Quate, C. *Adv. Mater.* **1999**, *11*, 314.
(8) Herr, D.; Zhirnov, V. *Solid State Technol.* **2004**, *47*, 26.
(9) Zhuravel, M.; Davis, N.; Nguyen, S.; Koltover, L. *J. Am. Chem. Soc.* **2004**, *126*, 9882.
(10) Haag, R.; Kratz, F. *Angew. Chem., Int. Ed.* **2006**, *45*, 1198−1215.
(11) Thissen, H.; Chang, K.; Tebb, T.; Tsai, W.; Glattauer, V.; Ramshaw, J.; Werkmeister, J. *J. Biomed. Mater. Res.* **2006**, *77A*, 590.
(12) Winston, O.; Marielle, G.; Angel, E. *Chem. Commun.* **2004**, 1677.
(13) Marchioni, F.; Venturi, M.; Credi, A.; Balzani, V.; Belohradsky, M.; Elizarov, A.; Tseng, H.; Stoddart, J. *J. Am. Chem. Soc.* **2004**, *126*, 568.
(14) Kotz, J.; Kosmella, S.; Beitz, T. *Prog. Polym. Sci.* **2001**, *26*, 1199.
(15) Li, Y.; Lin, S.; Goddard, W. *J. Am. Chem. Soc.* **2004**, *126*, 1872.
(16) Lin, S.; Jang, S.; Cagin, T.; Goddard, W. *J. Phys. Chem. B* **2004**, *108*, 10041.
(17) Götze, I. O.; Likos, C. N. *J. Phys.: Condens. Matter* **2005**, *17*, S1777.
(18) Hoffmann, N.; Likos, C.; Löwen, H. *J. Chem. Phys.* **2004**, *121*, 7009.
(19) Ulrich, S.; Seijo, M.; Stoll, S. *Curr. Opin. Colloid Interface Sci.* **2006**, *11*, 268.
(20) Tata, B.; Jena, S. *Solid State Commun.* **2006**, *139*, 562.
(21) Minko, S. *Polym. Rev.* **2006**, *46*, 397.
(22) de Vries, R.; Stuart, M. *Curr. Opin. Colloid Interface Sci.* **2006**, *11*, 295.
(23) Levin, Y. *Rep. Prog. Phys.* **2002**, *65*, 1577−1632.
(24) Levin, Y. *Physica A* **2005**, *352*, 43.
(25) Holm, C.; Joanny, J.; Kremer, K.; Netz, R.; Reineker, P.; Seidel, C.; Vilgis, T.; Winkler, R. *Adv. Polym. Sci.* **2004**, *166*, 67.
(26) Dijkstra, M. *Curr. Opin. Colloid Interface Sci.* **2001**, *6*, 372.
(27) Quesada-Perez, M.; Callejas-Fernandez, J.; Hidalgo-Alvarez, R. *Adv. Colloid Interface Sci.* **2002**, *95*, 295.
(28) Messina, R.; Holm, C.; Kremer, K. *Phys. Rev. Lett.* **2000**, *85*, 872.
(29) Cooper, C. L.; Dubin, P. L.; Kayitmazer, A. B.; Turksen, S. *Curr. Opin. Colloid Interface Sci.* **2005**, *10*, 52.
(30) Berret, J. *J. Chem. Phys.* **2005**, *123*, art. no. 164703.
(31) Karatasos, K.; Adolf, D. B.; Davies, G. R. *J. Chem. Phys.* **2001**, *115*, 5310.
(32) Forester, T.; Smith, W. CCLRC, Daresbury Laboratory, Daresbury, Warrington Wa4 4AD, England. The simulations were performed by utilization of an appropriately modified version of the DL_POLY package. DL_POLY is a parallel molecular dynamics package developed at Daresbury laboratory and is a property of the Council for the Central Laboratory of the Research Councils (CCLRC).
(33) Lee, I.; Athey, B.; Wetzel, A.; Meixner, W.; Baker, J. *Macromolecules* **2002**, *35*, 4510.
(34) Mayo, S.; Olafson, B.; Goddard III, W. *J. Phys. Chem.* **1990**, *94*, 8897.
(35) Karatasos, K. *Macromolecules* **2005**, *38*, 4472.
(36) Allen, M.; Tildesley, D. *Computer Simulation of Liquids;* Oxford Science Publications: New York, 1997.
(37) Lee, H.; Larson, R. *J. Phys. Chem. B* **2006**, *110*, 18204.
(38) Gurtovenko, A.; Lyulin, S.; Karttunen, M.; Vattulainen, I. *J. Chem. Phys.* **2006**, *124*, art. no. 094904.
(39) Accelrys, cerius 2 package.
(40) Nisato, G.; Ivkov, R.; Amis, E. *J. Macromolecules* **1999**, *32*, 5895.
(41) Nisato, G.; Ivkov, R.; Amis, E. *J. Macromolecules* **2000**, *33*, 4172.
(42) Huang, Q. R.; Dubin, P. L.; Moorefield, C. N.; Newkome, G. R. *J. Phys. Chem. B* **2000**, *104*, 898.
(43) Jang, J.; Bae, Y. *J. Chem. Phys.* **2002**, *116*, 3484.
(44) Osterod, F.; Kraft, A. *Chem. Commun.* **1997**, 1435−1436.
(45) Devadoss, C.; Bharathi, P.; Moore, J. *Angew. Chem., Int. Ed.* **1997**, *36*, 1633.
(46) Maiti, P.; Cagin, T.; Lin, S.; Goddard, W. *Macromolecules* **2005**, *38*, 979.
(47) Galperin, D. E.; Ivanov, V. A.; Mazo, M. A.; Khokhlov, A. R. *J. Polym. Sci., Ser. A* **2005**, *47*, 61.
(48) Terao, T. *Mol. Phys.* **2006**, *104*, 2507.
(49) Liu, M.; Kono, K. *J. Controlled Release* **2000**, *65*, 121.
(50) Fernandez, L.; Gonzalez, M.; Cerecetto, H.; Santo, M.; Silber, J. *Supramol. Chem.* **2006**, *18*, 633.
(51) Karatasos, K. *Macromolecules* **2006**, *39*, 4619.
(52) Hernandez-Rojas, J.; Wales, D. *J. Non-Cryst. Solids* **2004**, *336*, 218.
(53) Lee, J.; Elliott, S. *J. Non-Cryst. Solids* **1995**, *193*, 133.
(54) Billinge, S.; Thorpe, M. *Local Structure from Diffraction, Fundamental Materials Research*; Kluwer Academic Publishers: New York, 2002.
(55) Wilson, M.; Madden, P. *Phys. Rev. Lett.* **1994**, *72*, 3033.
(56) Stradner, A.; Sedgwick, H.; Cardinaux, F.; Poon, W.; Egelhaaf, S.; Schurtenberger, P. *Nature (London)* **2004**, *432*, 492.
(57) Hadjichristidis, N.; Pispas, S.; Floudas, G. *Block Copolymers: Synthetic Strategies, Physical Properties, and Applications;* John Wiley & Sons: New York, 2003.
(58) Harkless, C.; Singh, M.; Nagler, S.; Stephenson, G.; Jordan-Sweet, J. *Phys. Rev. Lett.* **1990**, *64*, 2285.
(59) Moreira, A.; Netz, R. *Phys. Rev. Lett.* **2001**, *87*, 078301.
(60) Naji, A.; Netz, R. *Eur. Phys. J. E* **2004**, *V13*, 43.
(61) Manning, G.; Ray, J. *J. Biomol. Struct. Dyn.* **1998**, *16*, 461.
(62) Netz, R. R. *Phys. Rev. Lett.* **2003**, *90*, 128104.
(63) Muthukumar, M. *J. Chem. Phys.* **2004**, *120*, 9343.
(64) Nguyen, T.; Grosberg, A.; Shklovskii, B. *Phys. Rev. Lett.* **2000**, *85*, 1568.

(65) Messina, R.; Gonzalez-Tovar, E.; Lozada-Cassou, M.; Holm, C. *Europhys. Lett.* **2002**, *60*, 383.
(66) Yua, Y.; Wu, J.; Gao, H. *J. Chem. Phys.* **2004**, *120*, 7223.
(67) Belloni, L. *J. Phys.: Condens. Matter* **2000**, *12*, R549.
(68) Chandler, D. *Introduction to Modern Statistical Mechanics*; Oxford University Press: Oxford, 1988.
(69) Linse, P. *J. Phys.: Condens. Matter* **2002**, *14*, 13449−13467.
(70) Feng, J.; Ruckenstein, E. *Colloids Surf. A* **2006**, *281*, 254.
(71) Allahyarov, E.; D'Amico, I.; Löwen, H. *Phys. Rev. Lett.* **1998**, *81*, 1334.
(72) Wu, J.; Bratko, D.; Prausnitz, J. *Proc. Natl. Acad. Sci. U.S.A.* **1998**, *95*, 15169.
(73) Larsen, A.; Grier, D. *Nature (London)* **1997**, *385*, 230.
(74) Angelini, T.; Golestanian, R.; Coridan, R.; Butler, J.; Beraud, A.; Krisch, M.; Sinn, H.; Schweizer, K.; Wong, G. *Proc. Natl. Acad. Sci. U.S.A.* **2006**, *103*, 7962.
(75) Linse, P.; Lobaskin, V. *Phys. Rev. Lett.* **1999**, *83*, 4208.
(76) Diehl, A.; Carmona, H.; Levin, Y. *Phys. Rev. E* **2001**, *64*, art. no. 011804.
(77) Löwen, H.; Allahyarov, E.; Likos, C.; Blaak, R.; Dzubiella, J.; Jusufi, A.; Hoffmann, N.; Harreis, H. *J. Phys. A: Math. Gen.* **2003**, *36*, 5827.
(78) Grønbech-Jensen, N.; Beardmore, K.; Pincus, P. *Physica A* **1998**, *261*, 74.

MA7019489